

A Strategy for Phase Identification of Precipitates in High Al-containing Austenitic and Ferritic Steels Using Electron Diffraction

Yoon-Uk Heo*

Graduate Institute of Ferrous Technology, Pohang University of Science and Technology, Pohang 790-784, Korea

*Correspondence to:
Heo YU,
Tel: +82-54-279-9036
Fax: +82-54-279-9079
E-mail: yunuk01@postech.ac.kr

Received December 6, 2014
Revised December 18, 2014
Accepted December 19, 2014

A strategy for phase identification of precipitates in high Al-containing austenitic and ferritic steels using electron diffraction (ED) is studied. Comparative studies of the various Al-containing precipitates (*k*-carbide, Ni₃Al, Fe₃Al, FeAl) show the similarities of crystal structure and lattice parameter. However, the slight differences of lattice parameter and structure display characteristic ED patterns (EDPs) which can be identified. L1₂ *k*-carbide and Ni₃Al can be differentiated by the length of \vec{g} (the reciprocal lattice vector), even though they show perfectly identical shapes of EDPs. DO₃ Fe₃Al and B₂ FeAl show the characteristic EDs in [110] and [112] beam directions due to the differences of Fe site occupancies in unit cells. *k*-carbide, Ni₃Al, and FeAl show also the similar EDs in [112], [112], and [110] beam directions, respectively. All the possible similarities of EDs among each phases and the strategy for phase identification are discussed on the bases of kinematical ED simulation.

Key Words: Electron diffraction pattern, B₂, DO₃, L1₂, *k*-carbide

INTRODUCTION

Rising energy and environmental demands request high Al alloying for weight reduction in the structural alloys. Al reduces the density of steels more than 10% per 1 wt% addition (Frommeyer et al., 2006). High weight reduction ability of Al is attractive in automobile industry. However, as Al contents increase more than 7 wt%, the alloys suffers serious embrittlement even in a ferritic region. Recent researches are focused on increasing Al-contents for low-density steels and preventing embrittlement caused by high Al-addition through the mixing of other alloy elements (Mn, Ni, Cr) (Palm, 2005). Additional advantage of Al alloying in steels is its strengthening effects of steels via solid solution hardening or precipitation of Al-bearing intermetallic compounds and carbide in the matrix. In heat resistant austenitic stainless steel and Ni-based super alloy, high Al-addition forms various intermetallic compounds (L1₂ Ni₃Al,

B₂ NiAl) and increases high temperature strength (Sourmail, 2001; Pollock & Tin, 2006). Besides the strengthening effect, superior corrosion resistance caused by the formation of a dense alumina protection layer is additional advantage in high Al-containing heat resistant austenitic stainless steels (Yanamoto et al., 2007).

High Al-addition in steels forms various precipitates including intermetallic compounds and carbides. In Mn-containing alloys, L1₂ *k*-carbide ((Fe, Mn)₃AlC), DO₃ (Fe, Mn)₃Al, and B₂ (Fe, Mn)Al are possible candidates. L1₂ (Fe, Ni)₃Al and B₂ (Fe, Ni)Al phases can precipitate in Ni-bearing alloys. When Mn and Ni are alloyed individually, these precipitates can be easily differentiated by the investigation of chemical composition using an energy dispersive X-ray spectroscopy or an electron energy loss spectroscopy. However, Mn and Ni are major alloying elements in high Al-containing alloys and most alloys have lots of Mn and Ni together. Carbon also makes phase identification more difficult by forming *k*-carbide. *k*-carbide

has the same structure with Ni_3Al . When fine precipitates are distributed in the matrix, phase identification through the chemical analysis is difficult due to the interference of the matrix. Carbon replication method is another solution, but coherent precipitates are hardly extracted. Carbon film also hinders the identification of k -carbide and intermetallic compounds. Demands for high alloying of Mn and Ni in low density steels make the condition for the phase identification hard.

In this study, a strategy for phase identification of precipitates in high Al-contained austenitic and ferritic steels using electron diffraction (ED) is introduced. Kinematical simu-

lation of ED patterns (EDPs) in Al-bearing precipitates is carried out and the solution for phase identification is discussed via comparative studies of EDPs on the various structures.

MATERIALS AND METHODS

Kinematical ED simulation of L1_2 k -carbide and Ni_3Al , DO_3 Fe_3Al , and B_2 FeAl is performed using 'crystal maker' software (CrystalMaker Software Ltd., UK). Unit cells of each structure are built from inorganic crystal structure database (ICSD). Detailed information of each phase is listed in Table 1.

Table 1. Lattice structures of precipitates in high Al-containing austenitic and ferritic steels

	k -carbide	Ni_3Al	Fe_3Al	FeAl
Lattice parameter (\AA)	3.857	3.571	5.791	2.908
Structurebericht name	L1_2	L1_2	DO_3	B_2
Space group	P_{m-3m}	P_{m-3m}	F_{m-3m}	P_{m-3m}
Prototype name	$(\text{Fe, Mn})_3\text{AlC}$	$(\text{Fe, Ni})_3\text{Al}$	$(\text{Fe, Mn})_3\text{Al}$	$(\text{Fe, Mn})\text{Al}$
Inorganic crystal structure database number	52913	71044	87136	87134

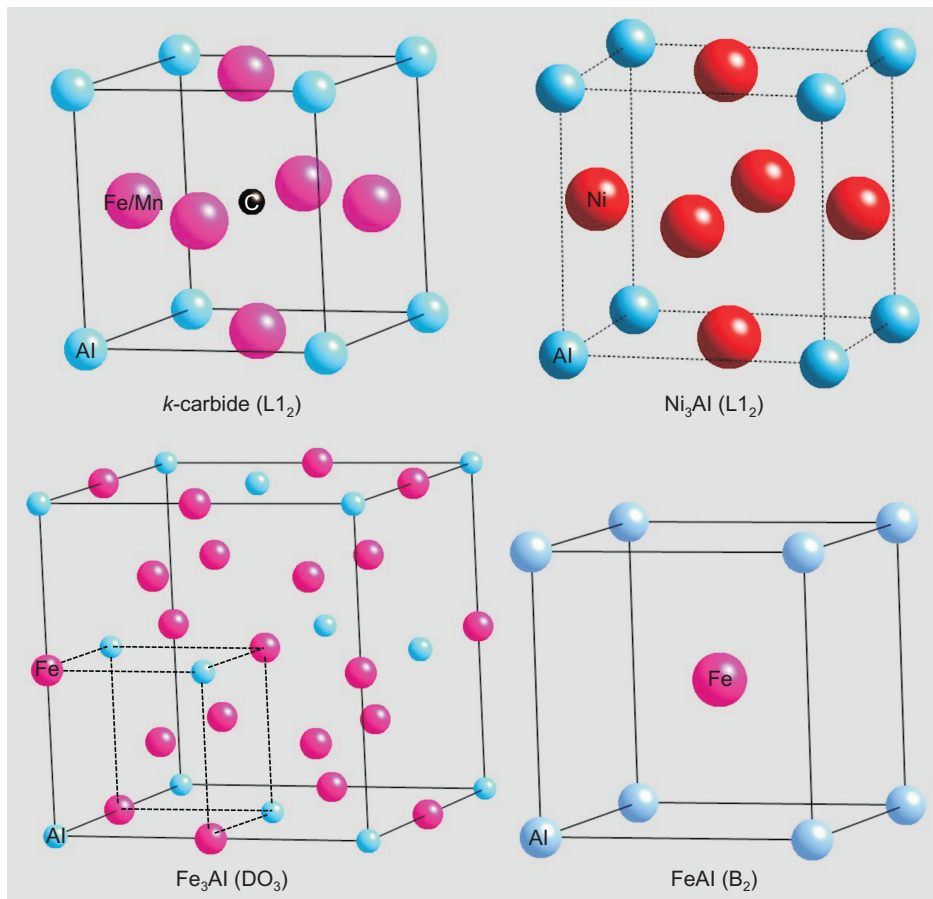


Fig. 1. Lattice structures of L1_2 k -carbide and Ni_3Al , DO_3 Fe_3Al , and B_2 FeAl .

Transmission electron microscope specimens of austenitic and ferritic high Al-containing steels were prepared by electropolishing in a universal solution (12% perchloric acid+88 acetic acid) maintained at 20°C and 51 V. The specimens were investigated in a JEM-2100F (JEOL, Japan) under an accelerating voltage of 200 kV.

RESULTS AND DISCUSSION

Fig. 1 shows lattice structures of $L1_2$ k -carbide and Ni_3Al , DO_3 Fe_3Al , and B_2 $FeAl$. k -carbide and Ni_3Al are a perfectly same structure except for a carbon in a body centered position of k -carbide. DO_3 Fe_3Al and B_2 $FeAl$ are also a similar body centered cubic structure. However, Fe_3Al and $FeAl$ show different atomic site occupancies. Fe and Al occupy in a body center and at the corner of an $FeAl$ unit cell, respectively. In Fe_3Al , Fe occupies half of 8 corners in addition to a body center in an $1/8$ unit cell. By the reason, Fe_3Al has two times larger lattice parameter than that of $FeAl$. Using lattice structures and information in Fig. 1 and Table 1, kinematical

ED simulation was performed. Simulated EDPs of each phase in low miller index zones are displayed in Fig. 2.

$L1_2$ k -carbide and $(Fe, Ni)_3Al$

As shown in Fig. 1, lattice structures of k -carbide and Ni_3Al are almost similar. Simulated shapes of EDPs in both phases are perfectly coincident in all beam directions (Fig. 2). Shapes of EDPs are not the hint for phase identification in this case. From the difference of lattice parameter between k -carbide ($a=3.857\text{\AA}$) and Ni_3Al ($a=3.571\text{\AA}$), we can draw a solution for phase identification. The length of \vec{g} , the reciprocal lattice vector, in both phases is slightly different in the simulated EDPs. The length of $\vec{g}_{001-k\text{-carbide}}$ is $1/3.86\text{ (\AA}^{-1}\text{)}$, but that of \vec{g}_{001-Ni_3Al} is $1/3.57\text{ (\AA}^{-1}\text{)}$. This length difference (7.5%) in \vec{g}_{001} can be detected when the microscope is well calibrated. Fig. 3 shows the experimentally obtained EDPs of k -carbide and $(Fe, Ni)_3Al$ precipitates in high Al-containing austenitic steels. EDPs were obtained from the same microscope where the camera constant is calibrated with Si single crystal. $[110]$ and $[112]$ EDPs of both phases look similar as we expected. However,

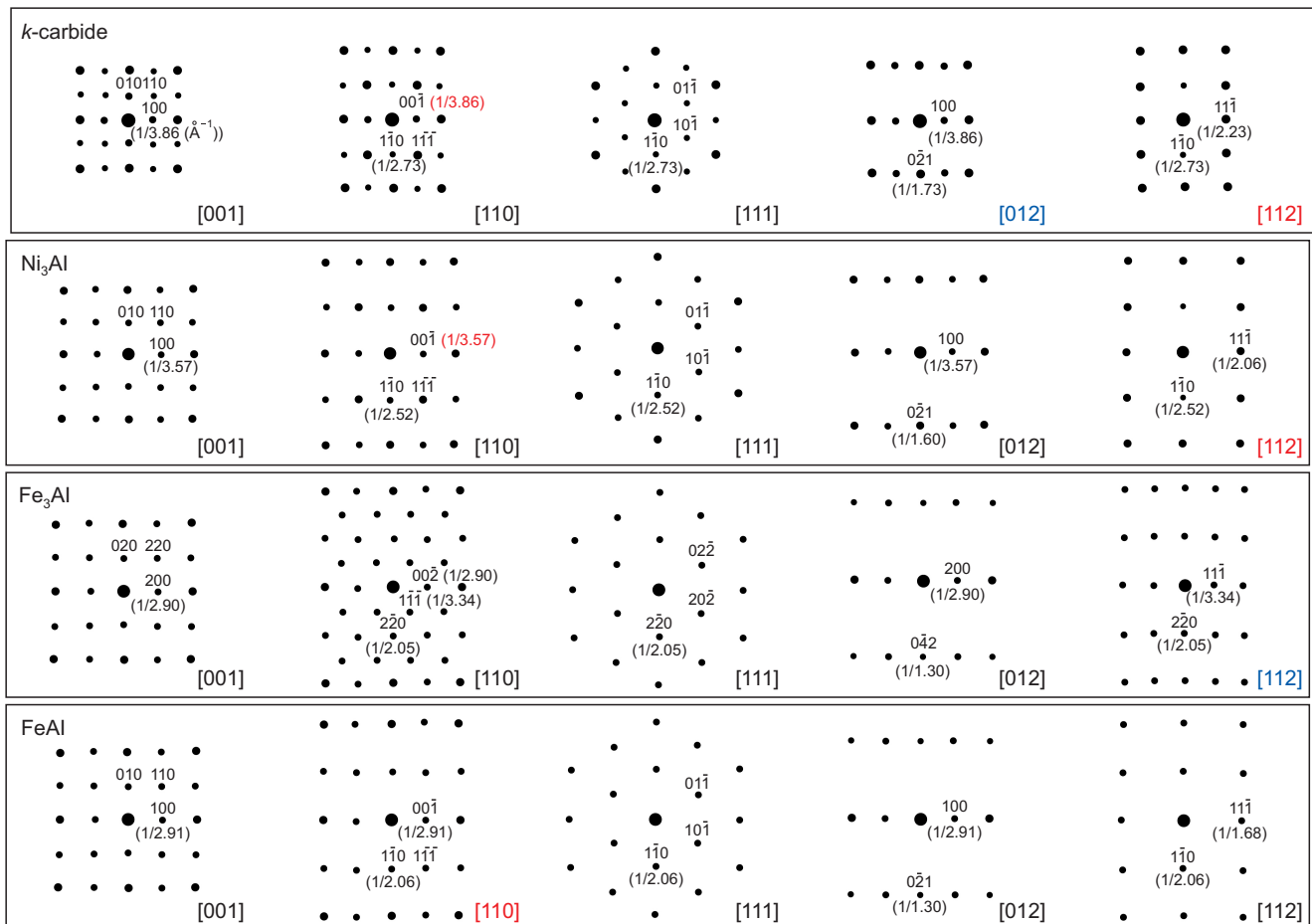


Fig. 2. Simulated electron diffraction patterns of $L1_2$ k -carbide and Ni_3Al , DO_3 Fe_3Al , and B_2 $FeAl$.

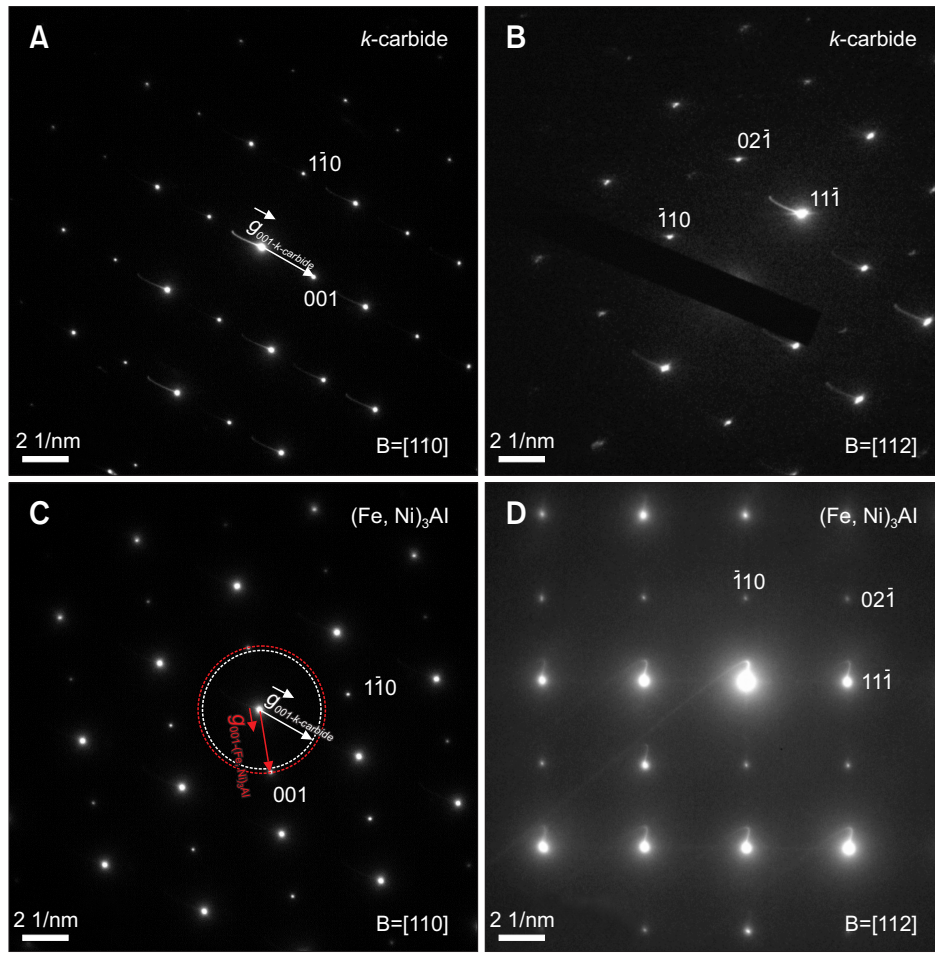


Fig. 3. Experimental electron diffraction patterns of *k*-carbide and (Fe, Ni)₃Al in high Al-containing austenitic steels (FeMnNiCrC-(8~10)Al based alloys). (A) [110]_{*k*-carbide} (B) [112]_{*k*-carbide} (C) [110]_{(Fe,Ni)₃Al} (D) [112]_{(Fe,Ni)₃Al} beam directions.

the length of $\vec{g}_{001-k\text{-carbide}}$ is shorter than that of \vec{g}_{001-Ni_3Al} due to large lattice parameter. For comparison, the circle which has a radius of $\vec{g}_{001-k\text{-carbide}}$ is superimposed in a [110] EDP of (Fe, Ni)₃Al (Fig. 3C). The difference of both circles which are composed of \vec{g}_{001} is clearly shown in Fig. 3C. In [112] pattern of both phases, this difference is also observed.

DO₃ (Fe, Mn)₃Al and B₂ (Fe, Mn)Al

Fe₃Al and FeAl have different atomic occupancies in a unit cell even though the basic structures of both phases are based on a body centered cubic structure. Simulated EDs of both phases show almost identical patterns except for [110] and [112] patterns. Lattice parameter of Fe₃Al is almost double of FeAl. The length of \vec{g} in Fe₃Al is half of that in FeAl. Most of EDPs in Fe₃Al and FeAl are perfectly coincident because of the existence of equivalent lattice planes. Phase identification is only possible by the comparative studies of both phases on [110] and [112] EDPs. Fe₃Al shows characteristic {111} types of spots in [110] EDP compared to the {111} spot positions in [110] EDP of FeAl. In [112] EDPs, {111}_{Fe₃Al} spots locate in half of $\vec{g}_{111-FeAl}$. Fig. 4 shows experimentally obtained [001]

and [110] EDPs of (Fe, Mn)Al and (Fe, Mn)₃Al precipitates in high Al-containing ferrite matrix. There is no difference in [001] EDPs of both phases (Fig. 4A and C). However, phase identification is possible in [110] EDPs due to {111} types of diffraction spots in (Fe, Mn)₃Al phase (Fig. 4D).

Additional Similarity of EDPs among Various Phases

Similarities of EDPs in L1₂ *k*-carbide and Ni₃Al, DO₃ Fe₃Al, and B₂ FeAl are identified in various beam directions because they have similar lattice structures and parameters. [001] and [111] EDPs of all the phases show perfectly coincident shapes of patterns. It is impossible to analyze each phase if the camera constant is not calibrated. In addition to [001] and [111] patterns, *k*-carbide and Fe₃Al have similar shape of EDPs in [012]_{*k*-carbide} and [112]_{Fe₃Al} beam directions. Close analysis on the \vec{g} length is needed for phase identification in this case. *k*-carbide, Ni₃Al, and FeAl have also similarity of EDPs in [112]_{*k*-carbide}, [112]_{Ni₃Al}, and [110]_{FeAl} beam directions, respectively. Careful analyses on the \vec{g} length are essential for phase identification.

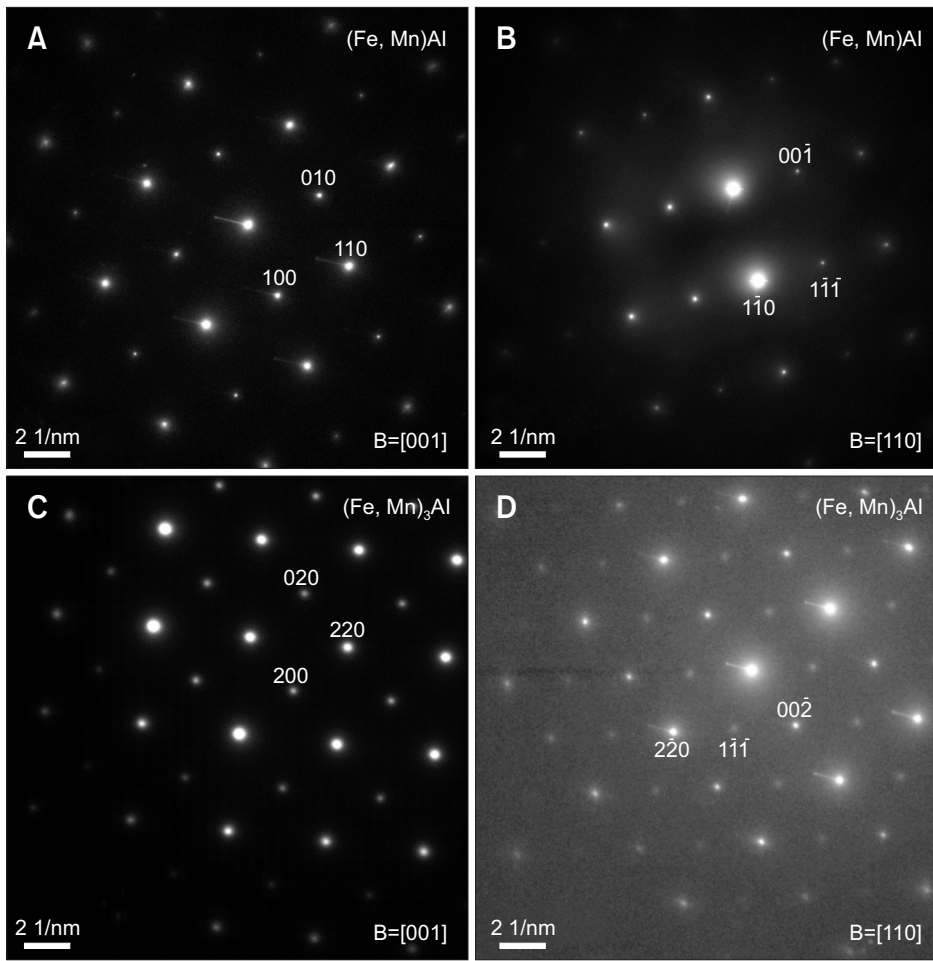


Fig. 4. Experimental electron diffraction patterns of (Fe, Mn)₃Al and (Fe, Mn)Al in high Al-containing ferrite matrix (FeMnC-(5-6)Al based alloys). (A) [001]_{Fe, MnAl} (B) [110]_{Fe, MnAl} (C) [001]_{Fe, MnAl} (D) [110]_{Fe, MnAl} beam directions.

Matrix Effects on the Precipitation Behavior of Each Phase

Precipitation behavior of second phase is closely related to the coherency between matrix and precipitates. *k*-carbide and austenite have a strong coherency due to the similar lattice parameter and structure. Cube to cube orientation relationship between *k*-carbide and austenite is reported (Lin et al., 2010). However, *k*-carbide shows Nishiyama-Wasserman relationship ($((110)_a // (111)_{k\text{-carbide}}, [001]_a // [10\bar{T}]_{k\text{-carbide}})$) with ferrite matrix (Seol et al., 2013). Fig. 5A and B show different morphologies of *k*-carbides precipitated in ferrite and austenite matrices. Precipitation of fine *k*-carbides is possible in austenite matrix due to similarity of lattice structures and parameters (Fig. 5B). *k*-carbides precipitated in ferrite matrix are coarse and frequently observed around the grain boundaries due to the lack of coherency (Fig. 5A). Interestingly, (Fe, Mn)₃Al show totally opposite precipitation behavior with that of *k*-carbide. (Fe, Mn)₃Al have a body centered cubic structure and similar lattice parameter with ferrite considered it's 1/8 unit cell (Fig. 1). (Fe, Mn)₃Al shows a good coherency with ferrite matrix. Austenite and (Fe, Mn)₃Al have a poor coherency. Fig. 5C and D are experimentally

observed images of (Fe, Mn)₃Al precipitates in ferrite and austenite matrices, respectively. Fine (Fe, Mn)₃Al precipitates are observed in ferrite matrix, and a coarse (Fe, Mn)₃Al particle is also confirmed in austenite matrix. To correct phase identification, these matrix effects on morphologies of precipitates should be also considered.

CONCLUSIONS

Based on the kinematical ED simulation on L1₂ *k*-carbide and Ni₃Al, DO₃ Fe₃Al, and B₂ FeAl precipitates, the strategy for phase identification using ED is proposed in high Al-containing austenitic and ferritic steels. Due to the structural similarity, each phase shows lots of similar EDPs. Present studies suggest that the accurate \vec{g} length measurement for L1₂ *k*-carbide and Ni₃Al precipitates, and the usages of [110] and [112] EDPs for DO₃ Fe₃Al and B₂ FeAl precipitates should be considered. Additional similarities in [012]_{*k*-carbide} and [112]_{Fe₃Al} and [112]_{*k*-carbide}, [112]_{Ni₃Al} and [110]_{FeAl} can be also overcome the correct \vec{g} length measurement. Finally, the effect of lattice coherency between precipitates and matrix (austenite, ferrite)

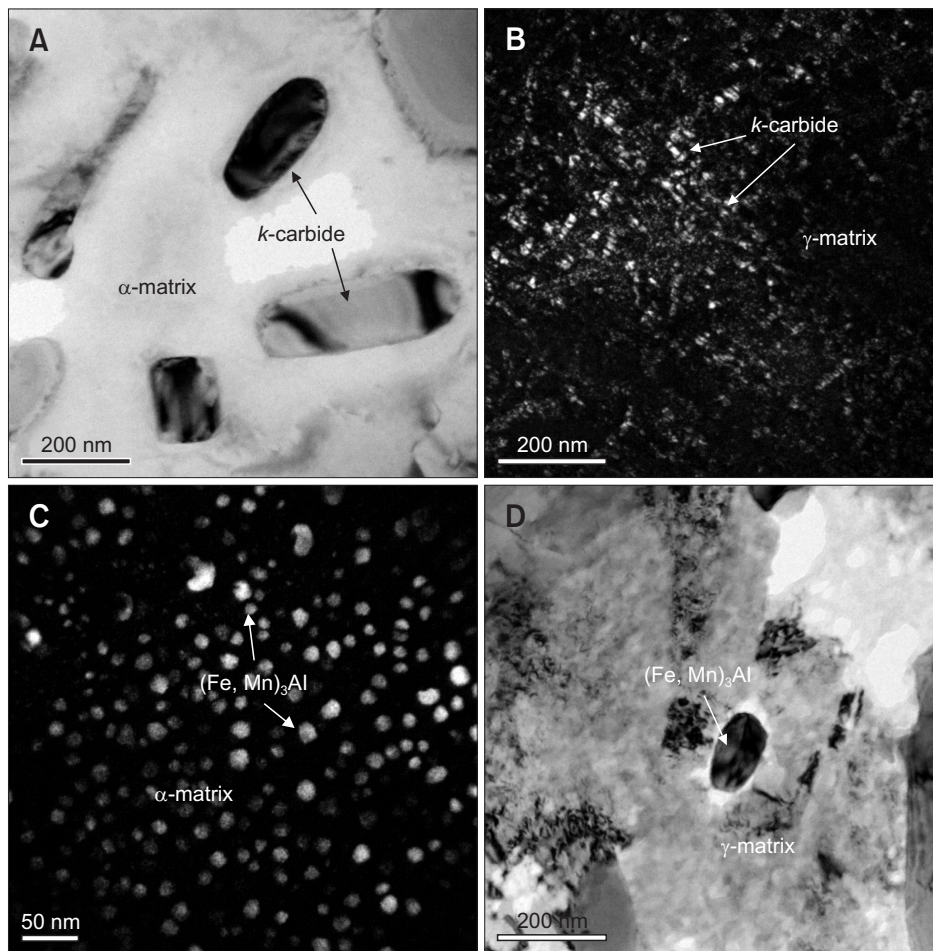


Fig. 5. Transmission electron microscope-bright field (BF) and dark field (DF) images of *k*-carbides and (Fe, Mn)₃Al particles precipitated in ferrite and austenite matrices. (A) BF image of *k*-carbide in ferrite matrix. (B) DF images of *k*-carbide in austenite matrix. (C) DF image of (Fe, Mn)₃Al in ferrite matrix. (D) BF image of (Fe, Mn)₃Al in austenite matrix.

on precipitation behavior was discussed. Morphologies of precipitates in each matrix are also additional information for the correct phase identification.

CONFLICT OF INTEREST

No potential conflict of interest relevant to this article was reported.

REFERENCES

- Frommeyer G, Drewes E J, and Engl B (2006) Physical and mechanical properties of iron-aluminium-(Mn, Si) lightweight steels. *J. Phys.* **10**, 1245-1253.
- Lin C L, Chao C G, Bor H Y, and Liu T F (2010) Relationship between microstructures and tensile properties of an Fe-30Mn-8.5Al-2.0C alloy. *Mat. Trans.* **51**, 1084-1088.
- Palm M (2005) Concepts derived from phase diagram studies for the strengthening of Fe-Al-based alloys. *Intermetallics* **13**, 1286-1295.
- Pollock T M and Tin S (2006) Nickel-based superalloys for advanced turbine engines: chemistry, microstructure, and properties. *J. Pro. Pow.* **22**, 361-374.
- Seol J B, Raabe D, Choi P, Park H S, Kwak J H, and Park C G (2013) Direct evidence for the formation of ordered carbides in a ferrite-based low-density Fe-Mn-Al-C alloy studied by transmission electron microscopy and atom probe tomography. *Scripta Mater.* **68**, 348-353.
- Sourmail T (2001) Precipitation in creep resistant austenitic stainless steels. *Mater. Sci. Tech.* **17**, 1-14.
- Yamamoto Y, Brady M P, Lu Z P, Liu C T, Takeyama M, Maziasz P J, and Pint B A (2007) Alumina-forming austenitic stainless steels strengthened by laves phase and MC carbide precipitates. *Met. Mat. Trans. A* **38**, 2737-2746.